Research Square

Preprints are preliminary reports that have not undergone peer review.
They should not be considered conclusive, used to inform clinical practice,
or referenced by the media as validated information.

White Matter Hyperintensity Burden Is Associated With Altered Functional Network Topology and Enhanced Structural-Functional Coupling in Cerebral Small Vessel Disease

Fan Yang
The First Affiliated Hospital of Shihezi University
Hanjiaerbieke Kukun
The First Affiliated Hospital of Xinjiang Medical University
Xiang Tan
The First Affiliated Hospital of Shihezi University
Tao Xiong
The First Affiliated Hospital of Shihezi University
Chao Guo
guochao7780163.com
The First Affiliated Hospital of Shihezi University

Research Article

Keywords: Cerebral small vessel disease, White matter hyperintensities, functional brain network, structural-functional coupling, resting-state functional MRI, diffusion tensor imaging, graph theory

Posted Date: July 14th, 2026

DOI: https://doi.org/10.21203/rs.3.rs-10192958/v1

License: This work is licensed under a Creative Commons Attribution 4.0 International License.
Read Full License

Additional Declarations: No competing interests reported.

White Matter Hyperintensity Burden Is Associated With Altered Functional Network Topology and Enhanced Structural-Functional Coupling in Cerebral Small Vessel Disease

Fan Yang[1], Hanjiaerbieke Kukun[2],Xiang Tan[1], Tao Xiong[1], Chao Guo[1*]

*Correspondence:
Chao Guo
guochao778@163.com
1 Medical Image Center, The First Affiliated Hospital of Shihezi University, Shihezi，No. 107, Community 32, North Second Road, Shihezi 832000, China
2 Department of Radiology, The First Affiliated Hospital of Xinjiang Medical University, No. 137, South Liyushan Road, Xinshi District, Ürümqi, Xinjiang, China

Abstract

Background Cerebral small vessel disease (CSVD) is commonly characterized by white matter hyperintensities (WMH), which may disrupt brain connectivity and contribute to cognitive and neurological impairment. This study investigated functional brain network topology and structural-functional coupling in CSVD patients with different WMH burdens.

Methods Patients with CSVD and healthy controls matched by age, sex, and education underwent brain MRI, cognitive assessment, and clinical evaluation. WMH severity was graded with the Fazekas scale, and CSVD patients were classified into low- and high-WMH-burden groups. Resting-state functional MRI was used to construct functional brain networks, and graph-theoretical methods were applied to quantify global and nodal topological properties. Diffusion tensor imaging was used to reconstruct structural brain networks. Whole-brain and regional structural-functional coupling values were derived from the correspondence between structural and functional connectivity matrices. Group differences were examined after adjusting for sex, age, and mean framewise displacement.

Results No significant intergroup differences were observed in key demographic characteristics or vascular risk profiles. Relative to healthy controls, the high-WMH-burden group exhibited significant alterations in global functional network topology, primarily manifested as higher clustering coefficient and increased normalized characteristic path length. Nodal analyses identified altered local network properties across visual, sensorimotor, frontal, and subcortical regions. Specifically, the high-WMH-burden group showed higher local network metrics in the left calcarine cortex, cuneus, superior occipital gyrus, paracentral lobule, and right middle frontal gyrus, together with reduced nodal local efficiency in the bilateral caudate nuclei. Whole-brain structural-functional coupling showed significant differences across the three groups and was higher in the high-WMH-burden group than in both healthy controls and the low-WMH-burden group. Regional coupling differences

were mainly located across temporal, frontal, insular, visual, and sensorimotor regions.

Conclusions Increased WMH burden in CSVD is linked to altered functional network topology and enhanced structural-functional coupling. These findings indicate that WMH-related white matter injury may drive brain network reorganization through increased local functional segregation and enhancing the dependence of functional activity on structural connectivity. Functional network metrics and structural-functional coupling measures may function as potential imaging markers for evaluating CSVD-related brain injury.

Keywords Cerebral small vessel disease; White matter hyperintensities; functional brain network; structural-functional coupling; resting-state functional MRI; diffusion tensor imaging; graph theory

Introduction

Cerebral small vessel disease (CSVD) comprises a group of clinical, imaging, and pathological syndromes affecting the cerebral small-vessel system, including small arteries, arterioles, capillaries, and venules. It is one of the most common forms of cerebrovascular disease in older adults[1]. In community-dwelling populations, the prevalence of CSVD increases substantially with age; among individuals aged 65 years or older, approximately 30% show severe white matter hyperintensities (WMH)[2]. CSVD can cause a broad spectrum of pathological changes, including chronic cerebral ischemia, white matter injury, lacunar infarction, and brain atrophy[3], and it is an important contributor to stroke, cognitive decline, gait impairment, mood disorders, and vascular dementia[4] .Because CSVD usually has an insidious onset and progresses gradually, some patients may present without overt clinical symptoms during the early stages. By the time cognitive or motor dysfunction becomes apparent, brain injury has often already reached a substantial level. Further investigation of the mechanisms underlying CSVD-related brain injury is therefore important for early disease identification, disease-severity assessment, and intervention for cognitive impairment.

WMH are a core imaging feature of CSVD. The pathological processes that underlie WMH involve structural and functional abnormalities of cerebral small vessels, leading to chronic ischemia and metabolic disturbance in white matter[1]. Blood-brain barrier (BBB) disruption is a key event in WMH development[5]. Previous studies have shown that BBB permeability is significantly increased in CSVD, especially in normal-appearing white matter (NAWM) and WMH regions[6]. A 4-year follow-up study of patients with hypertension showed that the progression of periventricular WMH was significantly related to cognitive performance, whereas baseline WMH burden exerted a comparatively limited effect on cognition[7]. WMH do not always progress continuously; lesion regression can occur in some patients, indicating that

the underlying pathological process may be potentially reversible[8].

In recent years, brain network research has provided a useful perspective for clarifying the pathophysiological mechanisms of CSVD. Cognitive and behavioral functions depend on coordinated neural activity across multiple brain regions, supported by the interaction between structural and functional connectivity. Conventional imaging assessments mainly focus on lesion number, volume, or distribution. Although these measures reflect the extent of focal brain injury, they cannot fully explain the heterogeneity of clinical manifestations in patients with CSVD. By contrast, brain network analysis allows system-level assessment of interregional connectivity patterns, information-transfer efficiency, and network organizational properties, thus providing a more integrated imaging framework for understanding cognitive impairment, motor dysfunction, and emotional changes in CSVD.

Resting-state functional magnetic resonance imaging (rs-fMRI) characterizes the synchronization of spontaneous neural across brain regions during rest and has become a key technique for investigating functional brain networks. The effect of WMH on brain function is not restricted to focal white matter lesions. Instead, WMH may disrupt interregional information-transfer pathways, alter whole-brain network organization, and ultimately contribute to cognitive decline[9]. Therefore, evaluating the effects of WMH severity on brain structure and function in CSVD from a brain network perspective may support a more comprehensive interpretation of CSVD-related brain injury and its clinical consequences. WMH in CSVD can cause abnormalities in resting-state brain network connectivity, mainly reflected in altered functional connectivity within the default mode network (DMN), executive control network, and corticostriatal network. A study of 116 patients with different degrees of WMH severity showed that individuals with greater WMH burden had increased DMN functional connectivity in the medial frontal gyrus but decreased connectivity in the thalamus. Notably, increased DMN functional connectivity in the medial frontal gyrus was independently linked to memory decline, whereas reduced DMN functional connectivity in the thalamus was independently linked to slower information processing speed[10].

Functional connectivity networks constructed from rs-fMRI data, together with graph-theoretical analysis of topological properties, can evaluate brain functional network alterations at both global and regional levels. In CSVD, greater WMH burden may be linked to reduced global efficiency, altered local connectivity, or changed network properties in key brain regions. A study of 36 patients with moderate-to-severe WMH reported that long-range functional connectivity in brain network network hubs, including the medial prefrontal cortex, precuneus, and thalamus, was significantly compromised. Moreover, the strength of long-range functional connectivity in the left dorsolateral prefrontal cortex was positively associated with information processing speed[11]. Beyond functional network

abnormalities, CSVD-related white matter injury may directly influence structural brain connectivity. White matter fiber tracts from the structural basis for interregional information transfer, and increased WMH burden may compromise the microstructural integrity of white matter,, resulting in weakened or disrupted anatomical connections between brain regions. Structural brain network analysis applies fiber tractography derived from diffusion tensor imaging (DTI) data to reconstruct white matter tracts and construct structural brain networks[12] .Previous studies have shown that patients with CSVD exhibit significant structural network abnormalities, including reduced network efficiency, decreased modularity, and impaired hub-node function[12].

Although previous studies have indicated that WMH are linked to cognitive decline and brain network abnormalities, several issues require further clarification. First, whether WMH burden causes abnormalities in the global topological organization of functional brain networks in CSVD remains uncertain. Second, whether patients with different levels of WMH burden show alterations in network properties within specific brain regions, and whether these alterations are associated with cognitive impairment, remains uncertain. Third, whether WMH contribute to abnormal coupling between structural and functional connectivity warrants further investigation.

Materials and Methods

Study Participants

Patients with CSVD who were treated at the First Affiliated Hospital of Shihezi University between November 2024 and March 2026 were included, and healthy controls matched by age, sex, and educational level were recruited over the same period. All participants underwent brain MRI, cognitive assessment, and collection of relevant clinical information, and all gave written informed consent.. This study was performed in accordance with the Declaration of Helsinki and approved by the Medical Ethics Committee of the First Affiliated Hospital of Shihezi University (approval No. KJ2025-538-02).

The eligibility criteria for patients with CSVD were as follows: (1) age between 50 and 80 years; (2) presence of relevant symptoms, including headache, dizziness, vertigo, limb numbness, gait instability, or cognitive decline; and (3) MRI evidence of CSVD-related imaging manifestations, such as WMH, enlarged perivascular spaces, lacunar infarcts, recent small subcortical infarcts, or cerebral microbleeds[13]. The exclusion criteria were as follows: large territorial cerebral infarction, traumatic brain injury, epilepsy, brain tumor, or history of intracerebral hemorrhage; concomitant severe neurological or psychiatric disorders; alcohol or drug abuse; history of radiotherapy or chemotherapy for malignant tumors; demyelinating diseases; conditions that may cause cognitive impairment, such as Alzheimer's disease or Parkinson's disease; acute complications related to type 2 diabetes mellitus or severe hypertension; obvious hearing, visual, or language impairment; and MRI

contraindications . The inclusion criterion for the control group was age between 50 and 80 years with no definite MRI features of CSVD. The exclusion criteria were identical to those applied to the CSVD group.

Clinical Data Collection and Scale Assessment

Demographic and clinical information was collected, including age, sex, educational level, smoking status, alcohol consumption, hypertension, diabetes mellitus, coronary heart disease, aortic atherosclerotic plaques, carotid plaques, fatty liver disease, blood glucose, lipid profiles, and body mass index (BMI). Educational level was scored based on the highest completed level of schooling: illiteracy, 1 point; primary school, 2 points; junior high school, 3 points; senior high school or technical secondary school, 4 points; and junior college, undergraduate education, or above, 5 points. Cognitive function was evaluated using the Montreal Cognitive Assessment (MoCA), with one additional point added to the total score for participants with fewer than 12 years of education[14]. Patients with severe dementia who could not cooperate with scale-based assessment were excluded.

White Matter Hyperintensity Assessment

WMH were independently evaluated by two experienced radiologists on FLAIR images with the Fazekas scale. When disagreement occurred, consensus was reached through discussion or adjudication by a third radiologist. The Fazekas score includes two components: periventricular WMH (PVWMH) and deep WMH (DWMH), each scored from 0 to 3, resulting in a total score of 0- 6. PVWMH was graded as follows: 0, absent; 1, caps or pencil-thin lining; 2, smooth halo; and 3, irregular hyperintensities extending into the deep white matter. DWMH was graded as follows: 0, absent; 1, punctate foci; 2, beginning confluence of lesions; and 3, large confluent areas. According to previous studies and Fazekas score cutoffs, patients with CSVD were stratified into a low-WMH-burden group (CSVD-LW; score, 1-2) and a high-WMH-burden group (CSVD-HW; score, 3-6)[15].

MRI Data Acquisition and Processing

MRI Image Acquisition

All participants underwent MRI on a Siemens 3T MAGNETOM Lumina scanner equipped with a 32-channel head coil. During scanning, participants were placed in the supine position and instructed to stay awake, keep their eyes closed, and avoid movement. Earplugs and foam pads were used to reduce acoustic noise and reduce motion artifacts. All participants first underwent MRI sequences required for CSVD diagnosis, and the imaging parameters are shown in **Table 1**.

Table 1 Brain MRI Sequences and Parameters

	T1WI	**T2WI**	**T2-FLAIR**	**DWI**	**T2WI-Sag**	**SWI**
TR（ms）	500	3230	8000	2800	3000	28
TE (ms)	6	126	97	76	97	20
FOV (mm)	220×220	230×230	230×230	230×230	240×240	220×220

Slice thickness（mm）	5	5	5	5	5	2
Number of slices	20	25	20	20	30	60

Axial DTI was obtained with the following parameters: repetition time (TR) , 4,800 ms; echo time (TE), 93 ms; 72 slices, slice thickness, 2 mm; field of view (FOV), 256 mm × 256 mm; b values, 0 and 1,000 s/mm², 30 diffusion-encoding directions; and simultaneous multi-slice (SMS) acceleration.
Axial rs-fMRI was obtained with the following parameters: TR,1,500 ms; TE, 30 ms; flip angle, 65°; 46 slices; FOV, 225 mm × 225 mm; slice thickness, 2.5 mm; no interslice gap; 240 time points; and SMS acceleration.
Structural T1-weighted images were acquired using a magnetization-prepared rapid gradient-echo (MPRAGE) sequence in the sagittal plane, covering the whole brain. The imaging parameters were as follows: TR = 1,610 ms, TE = 2 ms, flip angle = 8°, FOV = 256 mm × 256 mm, slice thickness = 1 mm, and number of slices = 384. The total scanning time was 35 min 56 s.

rs-fMRI Data Preprocessing
Preprocessing of rs-fMRI data was performed in GRETNA V2.0.0 implemented in MATLAB R2017a (http://www.nitrc.org/projects/gretna/)[16]. The main preprocessing workflow consisted of discarding the first five time points, correcting slice timing, correcting head motion, normalizing images to Montreal Neurological Institute (MNI) space with resampling to 2 mm × 2 mm × 2 mm voxels, linear detrending, regressing nuisance covariates, and applying band-pass filtering at 0.01 – 0.08 Hz. Nuisance covariates included white matter signals, cerebrospinal fluid signals, and 24 Friston head-motion parameters. Framewise displacement (FD) > 0.5 mm was defined as excessive instantaneous head motion. The affected volumes, together with one preceding and two subsequent volumes, were censored and replaced by nearest-neighbor interpolation. After preprocessing, mean FD showed no statistically significant difference among the groups (**Table 2**).

Functional Brain Network Construction and Graph-Theoretical Analysis
Functional brain networks were constructed in GRETNA. The automated anatomical labeling (AAL) atlas was usedparcellate the whole brain into 90 regions, which were used as network nodes. For each node, the mean blood oxygen level-dependent (BOLD) time series was extracted. Pearson correlation coefficients were then calculated for every pair of regions to form a 90 × 90 functional connectivity matrix for each participant. These coefficients were subsequently converted using *Fisher*'s z transformation and entered into the following statistical analyses.

Functional networks were thresholded using a sparsity-based strategy. To determine an appropriate sparsity interval, small-world properties were first examined across a candidate range from 0.05 to 0.50 at increments of 0.02. At each threshold, a network was regarded as having stable small-world topology when at least 90% of participants in every group simultaneously met $\gamma > 1.10$, $\sigma > 1.10$, and $0.90 \leq \lambda \leq 1.10$. The range

that jointly met these criteria in all three groups was 0.23–0.37 (**S 1**). Accordingly, 0.40 was selected as the maximum threshold at which small-world organization remained stable, and graph-theoretical indices were calculated across sparsity thresholds from 0.05 to 0.40 with an interval of 0.02.

Global graph-theoretical indices included the clustering coefficient (C_p), characteristic shortest path length (L_p), small-worldness (σ), global efficiency (E_g), local efficiency (E_{loc}), normalized characteristic path length (λ), and normalized clustering coefficient (γ). Regional nodal indices comprised nodal clustering coefficient (NCp), nodal efficiency (Ne), nodal degree centrality (NDC), nodal local efficiency (NLe), and betweenness centrality (Bc).

DTI Data Preprocessing and Structural Brain Network Construction

DTI preprocessing was conducted with PANDA 1.3.1 in a Linux environment. The preprocessing workflow included correction for eddy-current distortion, head-motion correction, and registration to the b0 image as the reference. Fiber tracking was performed with the fiber assignment by continuous tracking (FACT) algorithm. Tracking was stopped when the FA value was outside the range of 0.2-1.0 or when the turning angle between adjacent directions exceeded 45 ° . Diffusion tensor model-derived measures, including FA, were then calculated, and spatial registration was completed together with structural T1-weighted images.

For construction of the structural brain network, the AAL atlas was used to define 90 network nodes. The atlas was transformed into each participant's native DTI space, and the number of reconstructed fibers linking each pair of regions was used as the edge weight. Connections containing three or more fibers were retained as valid edges. A 90 × 90 fiber-number-weighted structural connectivity matrix was therefore obtained for each participant.

Structural–Functional Coupling Construction

Structural-functional coupling was estimated based on the AAL90 brain atlas. For each participant, the analysis used one 90 × 90 structural connectivity matrix and one 90 × 90 functional connectivity matrix. Before calculation, both matrices underwent quality-control procedures and symmetrization, and diagonal elements were set to zero. Whole-brain structural-functional coupling was derived by extracting the upper triangular elements of the two matrices and calculating the Spearman rank correlation coefficient between them. Regional structural-functional coupling was computed for each brain region by correlating its structural connectivity vector with its functional connectivity vector. In the primary analysis, only edges with structural connectivity strength higher than zero were retained. Group comparisons were conducted using a general linear model, with group as the main independent variable and sex, age, and mean framewise displacement (MeanFD) as covariates. For regional analyses, false discovery rate (*FDR*) correction was applied, and corrected q values < 0.05 were considered statistically significant.

Statistical Analysis

Continuous variables were summarized as medians with interquartile ranges [M (*P*25, *P*75)], and the Kruskal–Wallis *H* test was used for comparisons across the three groups. Categorical variables were summarized as n (%), and intergroup comparisons were conducted using the χ^2 test or *Fisher*'s exact test when the expected frequency was <5. Variables with a statistically significant overall group effect were further assessed by Bonferroni-corrected pairwise comparisons. Differences in graph-theoretical metrics among groups were examined using a general linear model/analysis of covariance. Each network metric was analyzed separately as the dependent variable, with group as the main independent variable, sex as a fixed factor, and age and meanFD as covariates. For metrics showing a significant main effect of group, post hoc pairwise comparisons were conducted with adjusted means.

Results

Participant Demographic and Clinical Characteristics

MoCA scores showed significant differences among the three groups ($H = 6.064$, $P = 0.048$). However, Bonferroni-corrected post hoc comparisons showed no significant differences between the HC and CSVD-LW groups, between the HC and CSVD-HW groups, or between the CSVD-LW and CSVD-HW groups (all adjusted $P > 0.05$). Age, educational level, BMI, glucose, triglycerides, total cholesterol, low-density lipoprotein cholesterol, and high-density lipoprotein cholesterol showed no significant difference among the three groups (all $P > 0.05$). Likewise, categorical variables, including sex, coronary heart disease, aortic atherosclerosis, carotid plaques, fatty liver disease, hypertension, diabetes mellitus, smoking status, and alcohol consumption, showed no statistically significant intergroup differences (all $P > 0.05$). (**Table 2**).

Table 2 DemographicandclinicalcharacteristicsofCSVDpatientsandcontrols

						p-Value(posthoc)		
Characteristics	**Controls**	**CSVD-LW**	**CSVD-HW**	***p*-Value**	***H/χ²/F***	**G1vsG2**	**G1vsG3**	**G2vsG3**
Age (years)	57.50（54.00, 61.25）	56.00（53.75, 62.00）	58.00（54.50, 61.00）	0.685	0.756[a]	-	-	-
Gender	M16/F20	M16/F24	M14/F25	0.752	0.57[b]	-	-	-
Educational score	3.00（3.00, 4.00）	3.00（3.00, 4.00）	3.00（2.00, 4.00）	0.562	1.154[a]	-	-	-
BMI	24.20（21.76, 28.00）	24.00（21.95, 27.04）	25.83（20.95, 29.00）	0.764	0.270[c]	-	-	-
MoCA	30.00（30.00, 30.00）	30.00（30.00, 30.00）	30.00（29.00, 30.00）	0.048	6.064[a]	0.999	0.118	0.086
GLU	4.82（4.50, 5.43）	5.24（4.67, 5.89）	4.80（4.59, 5.46）	0.067	5.400[a]	-	-	-
TAG	1.33（0.88, 1.99）	1.38（1.05, 2.50）	1.24（1.04, 2.05）	0.719	0.659[a]	-	-	-
LDL	2.50（1.99, 3.19）	2.78（2.31, 3.60）	2.89（2.29, 3.37）	0.319	2.284[a]	-	-	-
HDL	1.19（0.96, 1.34）	1.06（0.94, 1.42）	1.17（0.96, 1.35）	0.922	0.161[a]	-	-	-
CHD	10（27.8%）	13（32.5%）	13（33.3%）	0.857	0.309[b]	-	-	-
aortosclerosis,n (%)	6（16.7%）	10（25.0%）	9（23.1%）	0.659	0.835[b]	-	-	-
carotid plaque,n (%)	8（22.2%）	13（32.5%）	10（25.6%）	0.586	1.068[b]	-	-	-

Table 2 DemographicandclinicalcharacteristicsofCSVDpatientsandcontrols

Characteristics	Controls	CSVD-LW	CSVD-HW	*p*-Value	*H*/χ^2/*F*	*p*-Value(posthoc) G1vsG2	G1vsG3	G2vsG3
fatty liver,n (%)	9（25.0%）	13（32.5%）	13（33.3%）	0.692	0.738[b]	-	-	-
hypertension,n (%)	12（33.3%）	18（45.0%）	11（28.2%）	0.279	2.551[b]	-	-	-
diabetes,n (%)	1（2.8%）	4（10.0%）	4（10.3%）	0.396	1.853[d]	-	-	-
Smoking,n (%)	10（27.8%）	8（20.0%）	12（30.8%）	0.531	9.391[b]	-	-	-
drinking history,n (%)	4（11.1%）	4（10.0%）	6（15.4%）	0.744	4.383[d]	-	-	-
mean_FD	0.12（0.10，0.17）	0.11（0.08，0.16）	0.14（0.11，0.18）	0.350	2.098[a]	-	-	-

Abbreviations: G1,Controls; G2,CSVD-LW; G3,CSVD-LW;BMI, body mass index; MoCA, Montreal Cognitive Assessment; GLU, Glucose; TAG, Triglyceride; LDL,Low Density Lipoprotein; HDL, High-density lipoprotein; CHD,Coronary heart disease

[a] Kruskal-Wallis *H* test; [b] chi-square test;[c] *ANOVA* test;[d] Fisher's exact test

Topological Properties of Functional Brain Networks

Global Network Metrics

After adjusting for sex, age, and mean FD, *ANCOVA* was used to compare brain network topological metrics among the Controls, CSVD-LW, and CSVD-HW groups, followed by Bonferroni-corrected pairwise testing. Significant intergroup differences were observed in C_p, λ, and E_{loc}, and these differences were mainly located between the Controls and CSVD-HW groups. No significant intergroup differences were found in γ, L_p, σ, or E_g (**Table 3, Fig. 1**). Overall, these results indicate that the CSVD-HW group had evident alterations in selected global functional network metrics compared with the Controls group, whereas differences involving the CSVD-LW group were mild overall.

Table 3 Group comparisons of AUC values of global properties

Global property(AUC value)	Controls	CSVD-LW	CSVD-HW	*F*	Original *p*-value	*FDR*-corrected *p*-value	*p* value (post-hoc) G1 vs G2	G1vs G3	G2 vsG3
C_p	0.169±0.003	0.175±0.002	0.183±0.003	7.678	**0.001**	**0.005**	0.216	**0.001**	0.077
γ	0.599±0.015	0.623±0.014	0.619±0.015	0.721	0.488	0.570	0.767	0.999	0.999
λ	0.364±0.002	0.368±0.002	0.374±0.002	4.529	**0.013**	**0.045**	0.723	**0.011**	0.170
L_p	0.705±0.026	0.748±0.024	0.734±0.025	0.766	0.467	0.570	0.671	0.999	0.999
σ	0.555±0.014	0.569±0.013	0.558±0.014	0.343	0.710	0.710	0.999	0.999	0.999
E_g	0.181±0.003	0.176±0.002	0.174±0.002	1.981	0.143	0.250	0.420	0.177	0.999
E_{loc}	0.230±0.002	0.234±0.002	0.238±0.002	3.432	**0.036**	0.084	0.721	**0.031**	0.378

Abbreviations: AUC,area under the curve; *F*,*ANOVA* test; *FDR*, false discovery rate; E_g,global efficiency; E_{loc},local efficiency; C_p,clustering coefficient; γ, normalized clustering coefficient;λ,normalized characteristic path length; L_p,characteristic path length;σ,small-world attribute.

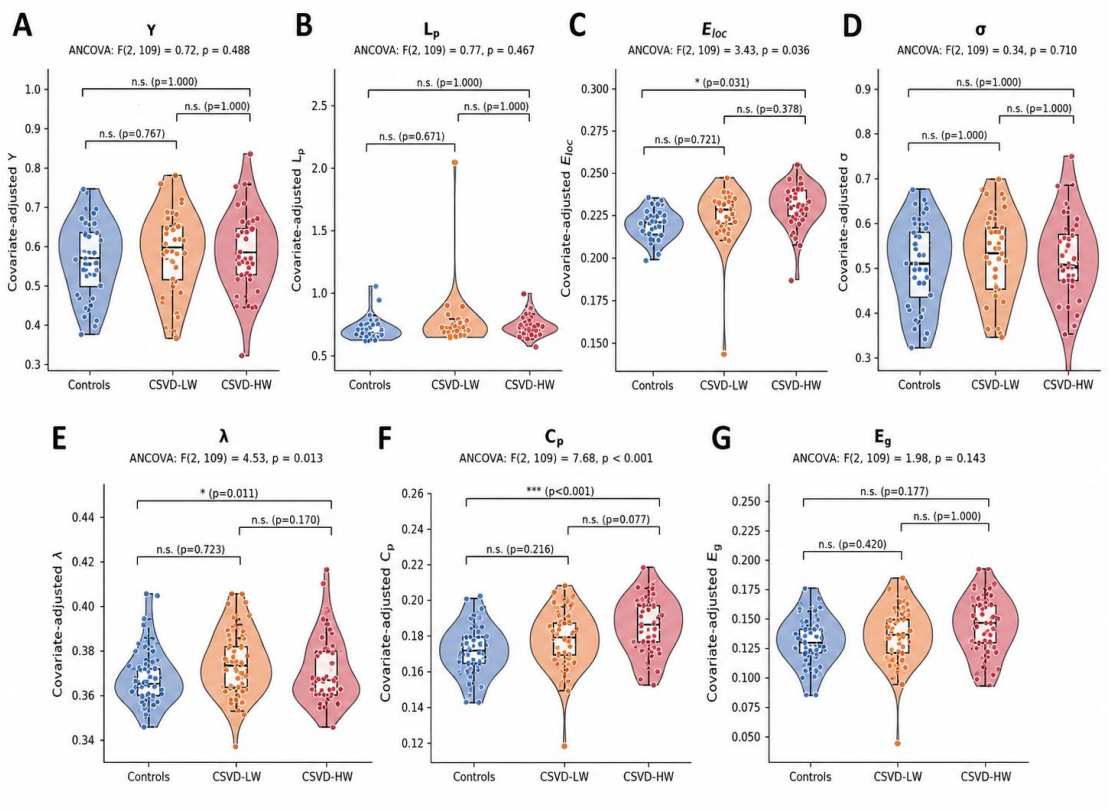

Fig. 1 Violin plots of brain network topological metrics among the Controls, CSVD-LW, and CSVD-HW groups. Notes: Violin plots showing the covariate-adjusted distributions of γ (A), L_p (B), E_{loc} (C), σ (D), λ (E), C_p (F), and E_g (G) among the three groups. Each dot represents an individual participant, and the box plot indicates the median and interquartile range. Between-group differences were assessed using analysis of covariance, with adjustment for sex, age, and mean_FD; pairwise comparisons were corrected using the Bonferroni method.

Analysis of Nodal Metrics

For NCpc, *ANCOVA* demonstrated significant intergroup differences after correction for multiple comparisons in the right middle frontal gyrus (MFG), superior occipital gyrus (SOG), left paracentral lobule (PCL), and bilateral calcarine fissure and surrounding cortex (CAL). Post hoc pairwise comparisons indicated that the CSVD-HW group showed the highest covariate-adjusted mean values in several nodes, while the left cuneus (CUN) represented a borderline node. Specifically, in the bilateral CAL and right SOG, values in the CSVD-HW group were significantly higher than those in both the Controls and CSVD-LW groups（**Table 4, Fig. 2**）.

Table 4 post-hoc pairwise comparisons after Holm correction

				G1 vs G2		G1 vs G3		G2 vs G3	
Node	**Region**	***F***	***p***	***t***	**Holm *p***	***t***	**Holm *p***	***t***	**Holm *p***
8	Frontal_Mid_R	6.951	0.001	-2.351	0.041	-3.697	0.001	-1.501	0.136
43	Calcarine_L	8.396	<0.001	-1.654	0.101	-4.060	0.001	-2.580	0.022
44	Calcarine_R	6.618	0.002	-0.770	0.443	-3.431	0.003	-2.812	0.012
50	Occipital_Sup_R	8.460	<0.001	0.111	0.912	-3.441	0.002	-3.709	0.001
69	Paracentral_Lobule_L	6.605	0.002	-1.845	0.109	-3.634	0.001	-1.943	0.109

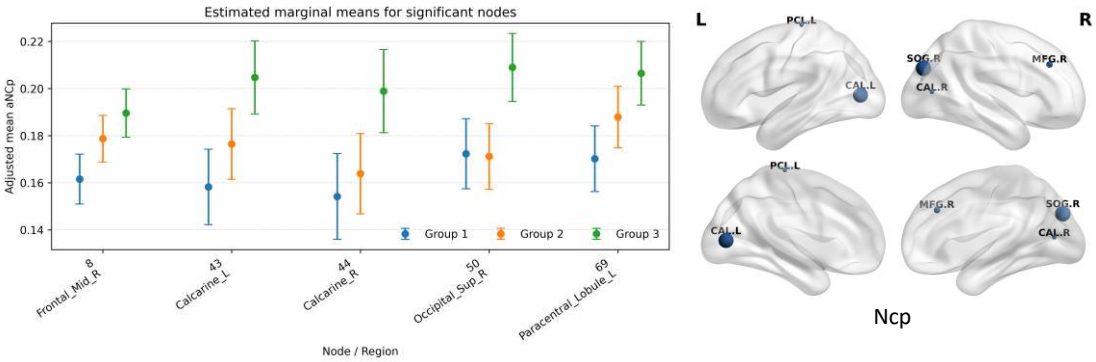

Fig. 2 Estimated marginal means of NCp for corrected significant nodes. Error bars indicate 95% confidence intervals after covariate adjustment.

For Ne, ANCOVA did not identify any nodes that simultaneously met both the GRETNA-corrected *p*-value threshold ($p < 0.001$) and the *F*-value threshold ($F > 11.119$). The right caudate nucleus (CAU) reached the corrected *p*-value threshold in the overall ANCOVA, but its *F* value lay at the boundary of the correction threshold(**S 2**).

For NLe, *ANCOVA* revealed significant intergroup differences after correction for multiple comparisons in five nodes, including the bilateral CAU, left CAL, CUN, PCL, and right SOG identified as a borderline node. Post hoc analyses showed that the CSVD-HW group had higher NLe values in the left CAL, CUN, and PCL than both the Controls and CSVD-LW groups. In contrast, NLe values in the bilateral CAU were significantly lower in the CSVD-HW group than in both comparison (**Table 5 , Fig. 3**).

Table 5 post-hoc pairwise comparisons after Holm correction

				G1 vs G2		G1 vs G3		G2 vs G3	
Node	**Region**	**F**	***p***	***t***	**Holm *p***	***t***	**Holm *p***	***t***	**Holm *p***
43	Calcarine_L	6.062	0.003	-1.143	0.255	-3.400	0.003	-2.404	0.035
45	Cuneus_L	6.161	0.003	-2.592	0.217	-3.375	0.003	-0.922	0.359
50	Occipital_Sup_R	6.019	0.003	-0.158	0.874	-3.033	0.009	-3.011	0.009
69	Paracentral_Lobule_L	6.026	0.003	-2.047	0.086	-3.460	0.002	-1.560	0.122
71	Caudate_L	6.223	0.003	-0.343	0.732	2.808	0.012	3.280	0.004
72	Caudate_R	7.623	<0.001	0.447	0.656	3.536	0.002	3.247	0.003

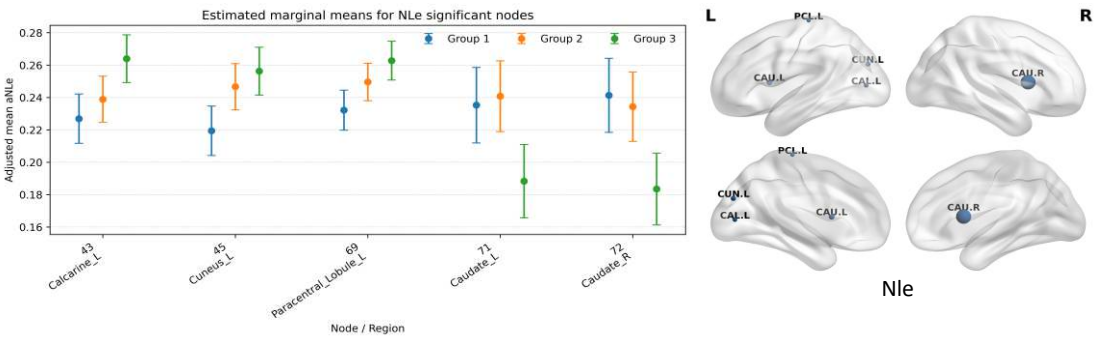

Fig. 3 Estimated marginal means of Nle for corrected significant nodes. Error bars indicate 95% confidence

intervals after covariate adjustment.

Structural-Functional Coupling Analysis

After controlling for sex, age, and mean head motion, whole-brain structural–functional coupling showed significant differences among the three groups (F = 11.080, $p < 0.001$). Pairwise comparisons further showed that whole-brain coupling was significantly higher in the CSVD-HW group than in the Controls group (β = 0.046, 95% CI: 0.026-0.067, $q < 0.001$) and the CSVD-LW group (β = 0.036, 95% CI: 0.016-0.055, $q < 0.001$). No significant difference was observed between the CSVD-LW and Controls groups (β = 0.011, q = 0.288) (**Table 6, Fig 4**).

Table 6 Group differences in global SC–FC coupling

Analysis	*β / F*	95% CI	*p* value	*FDR q* value
Overall group effect	F=11.080	—	<0.001	—
CSVD-LW vs Controls	0.011	−0.009 - 0.030	0.288	0.288
CSVD-HW vs Controls	0.046	0.026 - 0.067	<0.001	<0.001
CSVD-HW vs CSVD-LW	0.036	0.016 - 0.055	<0.001	<0.001

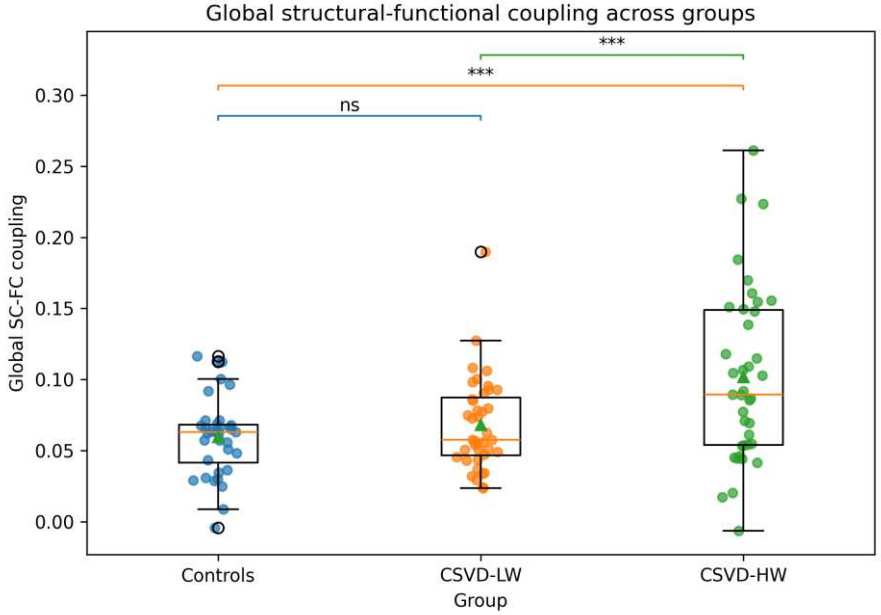

Fig. 4 Comparison of whole-brain structural-functional coupling among the Controls, CSVD-LW, and CSVD-HW groups.

Regional structural-functional coupling analysis demonstrated that, after FDR correction, 10 AAL90 regions showed significant overall between-group differences (**Table 7, Fig 5**). These regions included the the bilateral CAL, left rolandic operculum (ROL), left PCL, left superior temporal gyrus (STG), left insula (INS), right temporal pole of the superior temporal gyrus (TPOsup), right MFG, right TPOsup, and right medial superior frontal gyrus (SFGmed). Subsequent pairwise comparisons indicated that these regional differences were mainly attributable to the CSVD-HW group. Structural-functional coupling in the right TPOsup, right MFG and left ROL was higher in the CSVD-HW group than in both the Controls and CSVD-LW groups. Coupling in the left PCL was higher in both CSVD groups than in the Controls group, whereas no significant difference was observed between the two patient groups. In addition, the left CAL and right TPOsup mainly showed higher

coupling in the CSVD-HW group than in the CSVD-LW group, with the Controls group occupying an intermediate position.

Table 7 Brain regions showing significant group effects in regional structural-functional coupling

AAL90 brain region	*F* value	Overall *FDR q* value	CSVD-LW − Controls *β*（*q*）	CSVD-HW − Controls β（*q*）	CSVD-HW − CSVD-LW *β*（*q*）
Temporal_Pole_Sup_R	12.896	<0.001	0.020（0.950）	**0.238**（0.001）	**0.218**（0.004）
Rolandic_Oper_L	10.989	0.002	0.016（0.950）	**0.132**（0.002）	**0.115**（0.006）
Frontal_Mid_R	9.24	0.005	0.006（0.950）	**0.112**（0.006）	**0.107**（0.007）
Paracentral_Lobule_L	9.165	0.005	**0.201**（0.020）	**0.200**（0.007）	−0.001（0.995）
Calcarine_L	8.151	0.009	−0.060（0.759）	0.090（0.082）	**0.150**（0.005）
Temporal_Sup_L	7.052	0.02	0.075（0.418）	**0.148**（0.006）	0.073（0.194）
Temporal_Pole_Mid_R	6.906	0.02	−0.088（0.824）	0.199（0.082）	**0.287**（0.007）
Frontal_Sup_Medial_R	5.735	0.047	0.026（0.950）	**0.148**（0.025）	0.122（0.105）
Insula_L	5.628	0.047	0.010（0.950）	**0.084**（0.030）	0.074（0.096）
Calcarine_R	5.473	0.049	0.031（0.950）	**0.136**（0.025）	0.106（0.122）

Notes: Only AAL90 regions with significant FDR-corrected overall group effects are listed. *β* denotes the adjusted GLM estimate, with positive values indicating higher coupling in the former group. Values in parentheses are FDR-corrected *q* values for pairwise comparisons. Bold values indicate $q < 0.05$. L, left; R, right.

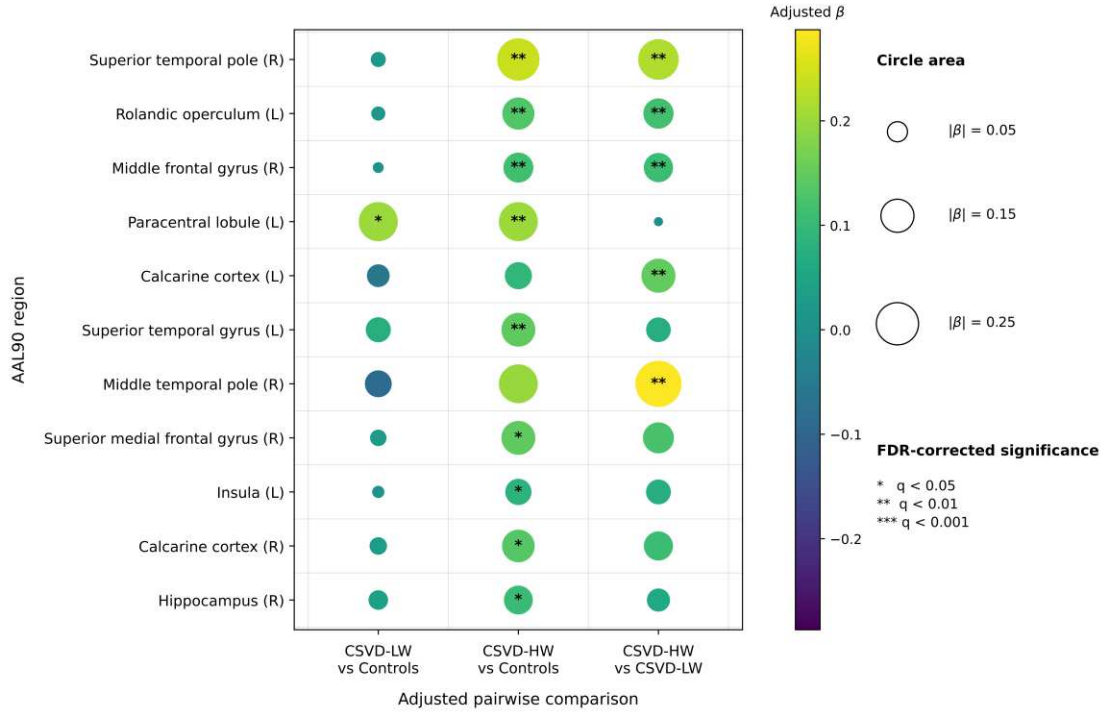

Fig. 5 Circular heatmap showing differences in regional structural-functional coupling among the three groups. Notes: Each row represents an AAL90 region, and each column represents a covariate-adjusted group comparison. Circle color indicates the direction and magnitude of *β*, and circle size indicates the absolute *β* value. Positive *β* indicates higher structural-functional coupling in the former group. Asterisks denote *FDR*-corrected significance. All models were adjusted for sex, age, and mean FD.

Discussion

The present study examined alterations in functional network topology and structural–

functional coupling in patients with CSVD stratified by WMH burden, using rs-fMRI, DTI, and graph-theoretical analysis. The main results showed no statistically significant differences among the three groups in age, sex, education level, blood glucose, blood lipids, body mass index, or major vascular risk profiles, indicating that baseline clinical characteristics were generally comparable. Although the overall difference in MoCA scores reached statistical significance, pairwise comparisons were not significant, indicating that cognitive impairment in this cohort was mild overall and may reflect an early stage of CSVD-related cognitive change. Network analysis showed that the high-WMH burden group exhibited more prominent abnormalities in global functional network topology, nodal properties, and structural–functional coupling, whereas differences between the low-WMH-burden group and healthy controls were comparatively limited.These findings suggest that increased WMH burden may serve as an important factor driver of brain network reorganization in CSVD.

High WMH Burden and Altered Global Functional Network Topology

For global functional network metrics, this study identified significant intergroup differences in C_p and λ, mainly between the CSVD-HW group and the healthy control group. The increased C_p in the CSVD-HW group suggests increased local clustering of the functional network and may reflect tighter local connectivity among neighboring or functionally related regions. Given the pathological basis of CSVD, WMH may impair long-range interregional information transfer through chronic ischemia, blood-brain barrier disruption, demyelination, and reduced integrity of white matter fiber pathways[17,18].When long-range connections are compromised, brain networks may increase local connectivity or local information processing to maintain functional stability to some degree[9]. Therefore, the increased C_p observed in the CSVD-HW group may reflect a compensatory form of network reorganization.

Meanwhile, the increased λ indicates that network integration efficiency may be impaired in the CSVD-HW group. λ reflects characteristic path length normalized to that of a random network; an increase in λ suggests relatively longer information-transfer pathways between brain regions and reduced whole-brain integration capacity[19]. Although Eg did not show a significant intergroup difference in the present study, the CSVD-HW group displayed enhanced local clustering and changes in path length-related metrics. These findings indicate that network abnormalities in CSVD may not simply be expressed as reduced overall efficiency, but rather as an altered balance between local segregation and global integration.

In this study, Eloc showed a trend toward group differences based on the uncorrected *P* value and in several pairwise comparisons, but these effects did not remain significant after *FDR* correction. Overall, functional network alterations in the CSVD-HW group were more consistent with a reorganization pattern characterized by strengthened local connectivity and restricted long-range integration.

Nodal Topological Alterations in Visual, Sensorimotor, and Frontal Regions

Further analysis of nodal metrics revealed altered local network properties in multiple regions in the CSVD-HW group, primarily involving the right MFG, bilateral CAL, right SOG, left CUN, and left PCL. The CAL, SOG, and CUN are primarily related to visual processing, whereas the PCL is closely linked to sensorimotor function. The right MFG participates in executive control, attentional regulation, and higher-order cognitive processing. These fresults suggest that influence of increased WMH burden on functional brain networks is not restricted to conventional cognitive networks, but also extend to visual, sensorimotor, and frontal executive-control regions.

For NCp, the CSVD-HW group showed higher values in nodes including the bilateral CAL, right SOG, and left PCL, indicating enhanced local clustering in these regions. Similarly, for NLe, the CSVD-HW group showed increased nodal local efficiency in the CAL, CUN, and PCL. This pattern may suggest that, under conditions of white matter injury, selected cortical regions offset impaired interregional connectivity by strengthening local information-processing capacity[20]. Notably, occipital visual regions and sensorimotor areas are key components of basic sensory and motor networks. Increased local efficiency in these regions may therefore reflect functional reorganization that supports the maintenance of basic sensory, motor, and visual information processing in patients with CSVD.

However, enhanced local network metrics do not necessarily indicate efficient compensation; they could also reflect maladaptive or inefficient network rearrangement. White matter injury in CSVD may disrupt coordinated activity among distributed brain regions and make network processing more reliant on local connections[21,22]. When local networks become excessively clustered while long-range connections remain insufficient, information-processing flexibility may decline, thereby affecting complex cognitive functions[23]. Thus, increased local metrics in occipital and sensorimotor-related regions may indicate a shift of network organization from distributed coordination toward more localized processing under high WMH burden.

Reduced Local Efficiency in the Bilateral CAU and Corticostriatal Circuit Impairment

In contrast with the increased local metrics observed in occipital and sensorimotor regions, NLe in the bilateral CAU was significantly lower in the CSVD-HW group than in both the control and CSVD-LW groups. The CAU is a key node within the cortico-striato-thalamo-cortical circuit and is closely related to executive function, attentional control, information-processing speed, and motor regulation[24]. Previous studies have suggested that CSVD-related cognitive impairment is often linked to disruption of frontal-subcortical circuits[25]. As a subcortical network hub, reduced CAU network efficiency may provide an important neural basis for cognitive and behavioral changes in patients with CSVD.

In this study, MoCA scores showed an overall intergroup difference, but pairwise comparisons were not statistically significant. Nevertheless, the median MoCA score in the CSVD-HW group was slightly lower than those in the control and CSVD-LW groups, suggesting a possible tendency toward mild cognitive decline. Together with the reduced local efficiency in the bilateral CAU, these findings indicate that early functional alterations in subcortical network nodes may already be present in patients with CSVD before marked deterioration in global cognitive performance becomes evident. Reduced CAU local efficiency may weaken information exchange with the frontal lobe, thalamus, and other cortical regions, thus providing a potential imaging explanation for later executive dysfunction, slowed processing speed, or gait abnormalities.

Enhanced Structural－Functional Coupling in the CSVD-HW Group

Another key finding of this study was that whole-brain structural-functional coupling was significantly higher in the CSVD-HW group than in both the control and CSVD-LW groups, whereas no significant difference was observed between the CSVD-LW and control groups. Structural-functional coupling reflects the relationship between structural and functional connectivity[26]. Under physiological conditions, functional activity in the healthy brain is constrained by structural connectivity while retaining a certain degree of dynamic flexibility[27]. The increased structural-functional coupling observed in the CSVD-HW group may suggest greater dependence of functional activity on the remaining structural connections, accompanied by reduced capacity for dynamic network regulation.

This finding may be interpreted from two complementary perspectives. First, increased WMH burden may compromise the integrity of white matter fibers and reduce the number or efficiency of long-range structural connections, thereby making functional connectivity more constrained by the remaining structural pathways and appearing as enhanced structural–functional coupling. Second, increased structural-functional coupling could also reflect compensatory reorganization. In the context of structural network damage, the brain may strengthen the correspondence between retained structural pathways and functional activity to maintain basic cognitive and behavioral performance[28,29]. However, excessive coupling may suggest insufficient functional network flexibility, limiting the capacity of the brain network to adapt effectively to task-related or environmental demands.

Regional structural-functional coupling analysis also revealed significant differences in several brain regions, including the right STG, left ROL, left PCL, right MFG, bilateral CAL, left STG, right MTG, right SFGmed, and left INS. These regions participate in multiple functional systems, including cognitive control, sensorimotor function, visual processing, language and semantic processing, and emotional and salience networks. Specifically, the right MFG, SFGmed, and INS are linked to higher-order cognitive control and attentional regulation[30]; the STG and TPOsup are associated with semantic processing, social cognition, and memory [31]; and the

CAL and PCL are involved in visual and sensorimotor functions, respectively [32,33]. These findings indicate that high WMH burden does not affect only a single brain region or network, but instead leads to alterations in structural-functional correspondence across multiple functional systems.

Notably, structural-functional coupling in the right STG, left ROL, and right MFG was higher in the CSVD-HW group than in both the healthy control and CSVD-LW groups, indicating that these regions may be particularly sensitive to increased WMH burden. Coupling in the left PCL was higher in both CSVD groups than in the healthy control group, indicating that structural–functional coupling abnormalities in this region may appear at an earlier stage of CSVD and may stabilize as WMH burden further increases. In contrast, coupling in the left CAL and right TPOsup was mainly higher in the CSVD-HW group than in the CSVD-LW group, indicating that alterations in these regions may be more dependent on the cumulative burden of WMH.

Implications for the Mechanisms of CSVD-Related Cognitive Impairment

By combining the findings on functional network topology and structural–functional coupling, this study suggests that patients in the CSVD-HW group exhibit multilayered brain network abnormalities. At the global level, enhanced local clustering and alterations in path length-related metrics indicate remodeling of brain network organization. At the nodal level, increased local network properties in occipital, sensorimotor, and frontal regions, together with reduced local efficiency in the CAU, suggest that cortical regions and subcortical nodes may undergo network alterations in different patterns. At the level of structural-functional relationships, increased whole-brain and regional structural-functional coupling in the CSVD-HW group suggests that functional brain activity may be more tightly constrained by structural connectivity, with a possible reduction in network flexibility.

These findings support the view that, as WMH burden increases, white matter fiber damage in patients with CSVD progressively worsens, leading to disruption of long-range structural and functional connections. In response, the brain may enhance local network connectivity and increase structural-functional correspondence to preserve basic function[34]. However, such reorganization may have limits. When enhanced localized connectivity occurs together with reduced efficiency of subcortical hubs, the overall coordination capacity of the brain network may gradually decline, thereby increasing risk of cognitive impairment, motor dysfunction, and emotional changes[35]. Therefore, topological properties of functional brain networks and structural-functional coupling metrics may function as potential imaging biomarkers for early identification and disease stratification of CSVD-related brain injury.

Study Limitations

This study has several limitations. First, this was a cross-sectional study, and therefore causal associations between increased WMH burden and brain network alterations

could not be established. Future longitudinal studies are needed to better characterize the dynamic relationships among WMH progression, brain network remodeling, and cognitive changes. Second, cognitive function in this study was evaluated mainly using the MoCA scale. Although the MoCA reflects global cognitive status, it has limited capacity to differentiate specific cognitive domains, such as executive function, information processing speed, attention, and memory. Future studies should include more comprehensive neuropsychological assessments to clarify associations between different brain network metrics and specific cognitive domains. Third, WMH burden was categorized using the Fazekas score. Although this approach is feasible in clinical practice, it offers limited quantitative precision regarding the spatial distribution and lesion volume of WMH relative to automated volumetric measurements. Future studies should integrate WMH volume, lesion spatial distribution, and white matter tract injury metrics to further verify the present findings. Fourth, structural network construction relied on DTI tractography, which may be affected by crossing fibers, tractography algorithms, and connection thresholds. Future studies using higher-angular-resolution diffusion imaging and multimodel tractography approaches may improve accuracy of structural connectivity measurements.

Conclusion

In summary, this study identified significant brain network abnormalities in the CSVD-HW group, mainly characterized by enhanced local clustering of functional networks, increased local network properties in several visual and sensorimotor-related brain regions, reduced local efficiency in the bilateral CAU and enhanced whole-brain and regional structural-functional coupling. These findings suggest that increased WMH burden may contribute to the development and progression of CSVD-related brain injury and cognitive changes through disruption of white matter structural connectivity, altering the topological organization of functional brain networks, and increasing the dependence of functional activity on structural pathways. Brain network topological metrics and structural-functional coupling measures may serve as important imaging markers for assessing the severity of CSVD-related brain injury and potential cognitive risk.

List of abbreviations

CSVD	Cerebral Small Vessel Disease
WMH	White Matter Hyperintensities
BBB	Blood Brain Barrier
NAWM	Normal-Appearing White Matter
rs-fMRI	resting-state functional Magnetic Resonance Imaging
DMN	Default Mode Network
DTI	Diffusion Tensor Imaging

BMI	Body Mass Index
MoCA	Montreal Cognitive Assessment
TR	Repetition Time
TE	Echo Time
FOV	Field of View
SMS	Simultaneous Multi-Slice
MNI	Montreal Neurological Institute
FD	Framewise Displacement
AAL	Automated Anatomical Labeling
NCp	Nodal clustering coefficient
Ne	Nodal efficiency
NDC	Nodal Degree Centrality
NLe	Nodal Local Efficiency
Bc	Betweenness centrality
FDR	False Discovery Rate
MFG	Middle Frontal Gyrus
SOG	Superior Occipital Gyrus
PCL	Paracentral Lobule
CAL	Calcarine Fissure and Surrounding Cortex
CUN	Cuneus
CAU	Caudate Nucleus
ROL	Rolandic Operculum
STG	Superior Temporal Gyrus
INS	Insula
TPOsup	Superior Temporal Gyrus
SFGmed	Medial Superior Frontal Gyrus

Declarations

Ethics approval and consent to participate

This research was conducted in accordance with the Declaration of Helsinki and was approved by the Medical Ethics Committee of the First Affiliated Hospital of Shihezi University.

All participants provided written consent for the publication of anonymized data collected during the study. No identifiable information about participants will be disclosed in this publication.

Competing interests

The authors declare no competing interests.

Author details

1 Medical Image Center, The First Affiliated Hospital of Shihezi University, Shihezi，No. 107, Community 32, North Second Road, Shihezi 832000, China

2 Department of Radiology, The First Affiliated Hospital of Xinjiang Medical University, No. 137, South Liyushan Road, Xinshi District, Ürümqi, Xinjiang, China

Acknowledgements

The authors thank all the staff and participants of this study for their important contributions.

Author contributions

All authors were involved in writing the above article. Fan Yang was responsible for the concept conception, investigation and the initial draft writing. Hanjiaerbieke Kukun was responsible for the verification of the text content. Tan Xiang was responsible for the organization of basic materials. Xiang Tan and Tao Xiong assisted in the collection of images. Chao Guo was responsible for the language polishing.

Funding

This research was supported by the Doctoral Fund Project of the First Affiliated Hospital of Shihezi University (BS2024009) and the Guiding Science and Technology Project of the Xinjiang Production and Construction Corps (2025ZD041).

Data availability

The datasets used during the current study are available from the corresponding author (Fan Yang) on reasonable request.

References

1. Shi Y, Wardlaw JM. Update on cerebral small vessel disease: a dynamic whole-brain disease. Stroke Vasc Neurol. 2016 Sep 1;1(3):83–92. doi:10.1136/svn-2016-000035

2. Lau AY, Mok V, Lee J, Fan Y, Zeng J, Lam B, et al. Retinal image analytics detects white matter hyperintensities in healthy adults. Ann Clin Transl Neurol. 2019 Jan 1;6(1):98–105. doi:10.1002/acn3.688

3. Yu W, Li Y, Hu J, Wu J, Huang Y. A study on the pathogenesis of vascular cognitive impairment and dementia: The chronic cerebral hypoperfusion hypothesis. J Clin Med. 2022 Aug 14;11(16):4742. doi:10.3390/jcm11164742

4. Rutten-Jacobs LCA, Rost NS. Emerging insights from the genetics of cerebral small-vessel disease. Ann N Acad Sci. 2020 Jul 1;1471(1):5–17. doi:10.1111/nyas.13998

5. Wardlaw JM, Smith C, Dichgans M. Mechanisms of sporadic cerebral small vessel disease: insights from neuroimaging. Lancet Neurol. 2013 May 1;12(5):483–97. doi:10.1016/S1474-4422(13)70060-7

6. Zhang CE, Wong SM, Haar HJ, Staals J, Jansen JFA, Jeukens CRLPN, et al. Blood-brain barrier leakage is more widespread in patients with cerebral small vessel disease. Neurology. 2017 Jan 31;88(5):426–32. doi:10.1212/WNL.0000000000003556

7. Uiterwijk R, Staals J, Huijts M, Leeuw PW, Kroon AA, Oostenbrugge RJ. MRI progression of cerebral small vessel disease and cognitive decline in patients with hypertension. J Hypertens. 2017 Jun 1;35(6):1263–70. doi:10.1097/HJH.0000000000001294

8. Leijsen EMC, Leeuw FE, Tuladhar AM. Disease progression and regression in sporadic small vessel disease-insights from neuroimaging. Clin Sci. 2017 Jun 1;131(12):1191–206. doi:10.1042/CS20160384

9. Meijer KA, Steenwijk MD, Douw L, Schoonheim MM, Geurts JJG. Long-range connections are more severely damaged and relevant for cognition in multiple sclerosis. Brain. 2020 Jan 1;143(1):150–60. doi:10.1093/brain/awz355

10. Chen X, Huang L, Ye Q, Yang D, Qin R, Luo C, et al. Disrupted functional and structural connectivity within default mode network contribute to WMH-related cognitive impairment. Neuroimage Clin. 2019 Jan 1;24:102088. doi:10.1016/j.nicl.2019.102088

11. Lu T, Wang Z, Zhu Y, Wang M, Lu CQ, Ju S. Long-range connections damage in white matter hyperintensities affects information processing speed. Brain Commun. 2024 Jan 1;6(1):fcae042. doi:10.1093/braincomms/fcae042

12. Robalo BM, Vlegels N, Meier J, Leemans A, Biessels GJ, Reijmer YD. Effect of fixed-density thresholding on structural brain networks: A demonstration in cerebral small vessel disease. Brain Connect. 2020 Apr 1;10(3):121–33. doi:10.1089/brain.2019.0686

13. Chen Weiqi, Xu Jiajie, Lu Yao, Wang Ling, Cao Jinyi, Chen Hongbin, et al. Neuroimaging Diagnostic Criteria and Standardized Definitions of Cerebral Small Vessel Disease in China: An Expert Consensus from the Chinese Stroke Society. Chinese Journal of Stroke. 2024;19(4):376–404. doi: 10.3969/j.issn.1673-5765.2024.04.002

14. Nasreddine ZS, Phillips NA, Bédirian V, Charbonneau S, Whitehead V, Collin I, et al. The Montreal Cognitive Assessment, MoCA: a brief screening tool for mild cognitive impairment. J Am Geriatr Soc. 2005 Apr 1;53(4):695–9. doi:10.1111/j.1532-5415.2005.53221.x

15. Zhu S, Qian S, Xu T, Peng H, Dong R, Wang D, et al. White Matter Hyperintensity, Immediate Antihypertensive Treatment, and Functional Outcome After Acute Ischemic Stroke. Stroke. 2020 May 1;51(5):1608–12. doi:10.1161/STROKEAHA.119.028841

16. Wang J, Wang X, Xia M, Liao X, Evans A, He Y. GRETNA: a graph theoretical network analysis toolbox for imaging connectomics. Front Hum Neurosci. 2015 Jan 1;9:386. doi:10.3389/fnhum.2015.00386

17. Reginold W, Sam K, Poublanc J, Fisher J, Crawley A, Mikulis DJ. Impact of white matter hyperintensities on surrounding white matter tracts. Neuroradiology. 2018 Sep 1;60(9):933–44. doi:10.1007/s00234-018-2053-x

18. Chen HF, Huang LL, Li HY, Qian Y, Yang D, Qing Z, et al. Microstructural disruption of the right inferior fronto-occipital and inferior longitudinal fasciculus contributes to WMH-related cognitive impairment. CNS Neurosci Ther. 2020 May 1;26(5):576–88. doi:10.1111/cns.13283

19. Sporns O. The non-random brain: efficiency, economy, and complex dynamics. Front Comput Neurosci. 2011 Jan 1;5:5. doi:10.3389/fncom.2011.00005

20. Xu F, Wang Y, Li H, Yu X, Wang C, Liu M, et al. Time-Varying Effective Connectivity for Describing the Dynamic Brain Networks of Post-stroke Rehabilitation. Front Aging Neurosci. 2022 Jan 1;14:911513. doi:10.3389/fnagi.2022.911513

21. Quandt F, Fischer F, Schröder J, Heinze M, Lettow I, Frey BM, et al. Higher white matter hyperintensity lesion load is associated with reduced long-range functional connectivity. Brain Commun. 2020 Jan 1;2(2):fcaa111. doi:10.1093/braincomms/fcaa111

22. Frey BM, Petersen M, Schlemm E, Mayer C, Hanning U, Engelke K, et al. White matter integrity and structural brain network topology in cerebral small vessel disease: The hamburg city health study. Hum Brain Mapp. 2021 Apr 1;42(5):1406–15. doi:10.1002/hbm.25301

23. Xu Y, Wang Y, Xu F, Li Y, Sun J, Niu K, et al. Impact of interictal epileptiform discharges on brain network in self-limited epilepsy with centrotemporal spikes: A magnetoencephalography study. Brain Behav. 2023 Jun 1;13(6):e3038. doi:10.1002/brb3.3038

24. Çırak M, Yağmurlu K, Kearns KN, Ribas EC, Urgun K, Shaffrey ME, et al. The Caudate Nucleus: Its Connections, Surgical Implications, and Related Complications. World Neurosurg. 2020 Jul 1;139:e428–38. doi:10.1016/j.wneu.2020.04.027

25. Sang L, Liu C, Wang L, Zhang J, Zhang Y, Li P, et al. Disrupted Brain Structural Connectivity Network in Subcortical Ischemic Vascular Cognitive Impairment With No Dementia. Front Aging Neurosci. 2020 Jan 1;12:6. doi:10.3389/fnagi.2020.00006

26. Baum GL, Cui Z, Roalf DR, Ciric R, Betzel RF, Larsen B, et al. Development of structure-function coupling in human brain networks during youth. Proc Natl Acad Sci U A. 2020 Jan 7;117(1):771–8. doi:10.1073/pnas.1912034117

27. Deco G, Jirsa VK, McIntosh AR. Emerging concepts for the dynamical organization of resting-state activity in the brain. Nat Rev Neurosci. 2011 Jan 1;12(1):43–56. doi:10.1038/nrn2961

28. Zhang X, Liang C, Wang N, Wang Y, Gao Y, Sui C, et al. Abnormal whole-brain voxelwise structure-function coupling and its association with cognitive dysfunction in patients with different cerebral small vessel disease burdens. Front Aging Neurosci. 2023 Jun 30;15:1148738. doi:10.3389/fnagi.2023.1148738

29. Tay J, Düring M, Van Leijsen EMC, Bergkamp MI, Norris DG, De Leeuw FE, et al. Network structure-function coupling and neurocognition in cerebral small vessel disease. NeuroImage Clin. 2023;38:103421. doi:10.1016/j.nicl.2023.103421

30. Lopes R, Bournonville C, Kuchcinski G, Dondaine T, Mendyk AM, Viard R, et al. Prediction of long-term cognitive function after minor stroke using functional connectivity. Neurology. 2021 Feb 22;96(8):e1167–79. doi:10.1212/WNL.0000000000011452

31. Yi HG, Leonard MK, Chang EF. The Encoding of Speech Sounds in the Superior Temporal Gyrus. Neuron. 2019 Jun 19;102(6):1096–110. doi:10.1016/j.neuron.2019.04.023

32. Chen C, Jiang WH, Wang W, Ma XC, Li Y, Wu J, et al. Impaired visual, working, and verbal memory in first-episode, drug-naive patients with major depressive disorder in a Chinese population. PLoS One. 2018 Jan 1;13(4):e0196023. doi:10.1371/journal.pone.0196023

33. Jiang X, Fu S, Yin Z, Kang J, Wang X, Zhou Y, et al. Common and distinct neural activities in frontoparietal network in first-episode bipolar disorder and major depressive disorder: Preliminary findings from a follow-up resting state fMRI study. J Affect Disord. 2020 Jan 1;260:653–9. doi:10.1016/j.jad.2019.09.063

34. Krohn S, Schwanenflug N, Waschke L, Romanello A, Gell M, Garrett DD, et al. A spatiotemporal complexity architecture of human brain activity. Sci Adv. 2023 Feb 3;9(5):eabq3851. doi:10.1126/sciadv.abq3851

35. Tuladhar AM, Uden IWM, Rutten-Jacobs LCA, Lawrence A, Holst H, Norden A, et al. Structural network efficiency predicts conversion to dementia. Neurology. 2016 Mar 22;86(12):1112–9. doi:10.1212/WNL.0000000000002502

Supplementary Files

This is a list of supplementary files associated with this preprint. Click to download.

- S1.xls
- S2.doc